
HIERARCHICAL ATTENTION VIA DOMAIN DECOMPOSITION

A PREPRINT

Stephan Köhler and Oliver Rheinbach

Faculty of Mathematics and Computer Science
Technische Universität Bergakademie Freiberg, 09596 Freiberg, Germany

June 18, 2026

Abstract

We propose a hierarchical attention mechanism based on two-level overlapping Schwarz domain decomposition. The method is motivated by the observation that two-level Schwarz domain decomposition methods combine local subdomain corrections with a coarse level that communicates global, long-range information. We test its usefulness in the context of finite-dimensional operator learning using a simple, one-dimensional diffusion problem with homogeneous Dirichlet boundary conditions. Although elementary, this problem provides a controlled sequence-to-sequence setting in which the exact nonlocal solution operator is known. After discretization, learning the solution operator amounts to approximating the inverse of a symmetric positive definite matrix. As a baseline, we use a global softmax-free low-rank attention operator of the form QK^T . The proposed construction replaces this dense global factorization by a two-level additive structure: local low-rank attention blocks on overlapping subdomains are combined with a coarse attention block. The resulting operator has the form

$$M_\theta^{-1} = \Phi Q_0 K_0^T \Phi^T + \sum_{i=1}^N R_i^T D_i^{1/2} Q_i K_i^T D_i^{1/2} R_i.$$

Here R_i restricts to an overlapping subdomain, D_i is a partition-of-unity weight, and Φ is a coarse interpolation (or prolongation) matrix. Numerical experiments for synthetic Fourier right-hand sides indicate that the domain-decomposition attention operator is able to train faster and can give more accurate approximations than a global low-rank attention baseline while using significantly fewer parameters.

1 Introduction

The introduction of the attention mechanism in [1] has been central to the success of modern large language models. Unlike earlier recurrent networks, attention enables the direct and parallel modeling of contextual dependencies across long sequences. Formally, attention can be understood as a family of learnable interaction operators whose applicability arises from the exploitation of low-rank factorizations in the computation of token interactions.

A standard self-attention layer starts from an input matrix

$$X \in \mathbb{R}^{n \times d_{\text{in}}},$$

where the rows correspond to n tokens, grid points, or degrees of freedom, and the d_{in} columns contain the associated features. The query, key, and value matrices are obtained by learned linear mappings,

$$Q = XW_Q, \quad K = XW_K, \quad V = XW_V, \tag{1}$$

$$W_Q, W_K \in \mathbb{R}^{d_{\text{in}} \times d_k}, \quad W_V \in \mathbb{R}^{d_{\text{in}} \times d_v}.$$

The standard, scaled dot-product attention operator with softmax is then

$$\text{Att}_{\text{softmax}}(X) = \text{softmax}\left(\frac{QK^T}{\sqrt{d_k}}\right)V,$$

where d_k is the number of columns of W_Q and W_K . The operator softmax is the row-wise application of softmax, i.e., for a matrix G

$$(\text{softmax}(G))_{ij} = \frac{\exp(G_{ij})}{\sum_{\ell=1}^n \exp(G_{i\ell})}.$$

The matrix $QK^T \in \mathbb{R}^{n \times n}$ contains pairwise interactions between the n tokens or, in our case, grid points. The parameter d_k corresponds to the rank r of the low-rank factorization QK^T , i.e.,

$$r = \text{rank}(QK^T) \leq d_k.$$

In this work, we will omit the softmax operator. We also omit the scaling by $\sqrt{d_k}$, which arises from the fact that the diagonal of QK^T is the scalar product of vectors of length d_k . This scaling was introduced to improve the optimization by stochastic gradient descent or variants thereof such as Adam [2].

In total, we have the linear attention operator

$$\text{Att}(X) = (QK^T)V.$$

Remark 1 *Numerical analysts may find a column-vector convention more convenient, i.e., to write (1) as $Q^T = W_Q^T X^T$, $K^T = W_K^T X^T$, $V^T = W_V^T X^T$, where data points are now columns in X^T , features are rows in X^T , and the learnable weight matrices W_Q^T, W_K^T, W_V^T act from the left.*

Summarizing, in this work, we consider a setting in which the attention operator is softmax-free and thus linear, and trained to approximate a known solution operator in the sense of finite-dimensional operator learning. This allows to focus on the question if methods from numerical domain decomposition [3–5] can be used to design more efficient attention operators.

Our model problem is a discretized one-dimensional Poisson problem. After discretization, the solution map is the inverse of the sparse system matrix. A global low-rank attention layer can represent a rank- d_k approximation of this inverse. However, elliptic inverses have multiscale structure: local coupling is most important, but long-range low-frequency components must also be represented. This is the structure exploited, e.g., by two-level Schwarz domain decomposition methods [3–5] for partial differential equations.

We introduce a two-level attention mechanism inspired by overlapping Schwarz domain decomposition. The fine level consists of local low-rank attention blocks on overlapping subdomains. The coarse level consists of an attention block acting on a small interface-hat coarse basis. The construction is not meant as a replacement for classical solvers. Rather, it is a controlled experiment to demonstrate that domain decomposition concepts can provide a useful structure, e.g., for operator learning methods [6–8] or natural language processing. Modern overlapping Schwarz methods are highly parallel scalable methods in the solution of partial differential equations, e.g., [9, 10].

In the context of natural language processing (NLP) and large language models (LLMs), our one-dimensional Poisson problem, presented in section 2, can be interpreted as a sequence of tokens, where the local interactions between neighboring tokens are strongest. However, weaker long-range dependencies must also be represented. In our two-level Schwarz attention, the coarse level represents the weaker long range interactions while strong local interactions are captured by the overlapping subdomains.

We note that hierarchical forms of attention have been studied previously in different settings [11–13]. These approaches are not directly comparable to the one proposed here, since both the underlying mechanisms and the intended applications are different. In the present work, the hierarchy is induced by an overlapping domain decomposition and is used to structure a softmax-free attention approximation of elliptic solution operators. Hierarchical methods in NLP include [14–17].

After completion of this manuscript, we found that our approach to operator learning with linear attention has close connections to the work [18], where attention is used for operator learning.

2 One-Dimensional Diffusion Model Problem

We consider the Poisson problem in one dimension

$$-u''(x) = f(x), \quad x \in (0, 1) \subset \mathbb{R}^1, \quad u(0) = u(1) = 0. \quad (2)$$

Let $n + 2$ be the number of grid points, then n is the number of interior grid points and let

$$x_j = \frac{j}{n+1}, \quad j = 1, \dots, n. \quad (3)$$

Using the standard finite difference or finite element discretization gives

$$Au = f, \quad A = \frac{1}{h^2} \begin{pmatrix} 2 & -1 & & & \\ -1 & 2 & -1 & & \\ & \ddots & \ddots & \ddots & \\ & & -1 & 2 & -1 \\ & & & -1 & 2 \end{pmatrix}, \quad h = \frac{1}{n+1}. \quad (4)$$

The exact discrete solution operator is therefore

$$f \mapsto u = A^{-1}f. \quad (5)$$

The learning task in this paper is to approximate A^{-1} by a trainable structured operator M_θ^{-1} , where θ denotes the parameters.

For our one-dimensional model problem, a typical choice for the input matrix X is

$$X = \begin{pmatrix} x_1 & f_1 \\ x_2 & f_2 \\ \vdots & \vdots \\ x_n & f_n \end{pmatrix} \in \mathbb{R}^{n \times 2},$$

i.e., X contains the local grid points and the right-hand side as features.

However, for us, instead of using the physical coordinates as an input feature, it is more convenient to represent the grid points by a one-hot encoding and augment this representation by the right-hand side f , i.e., our feature matrix is

$$X = [I_n, f] \in \mathbb{R}^{n \times (n+1)}.$$

Thus, $d_{\text{in}} = n + 1$, i.e., the first n columns identify the grid points, while the last column contains the values of the right-hand side f .

Next, the weight matrix W_V is chosen as a fixed matrix which extracts the right-hand side channel from X , i.e.,

$$V = XW_V = f \in \mathbb{R}^{n \times 1}, \quad W_V = \begin{pmatrix} 0 \\ 1 \end{pmatrix},$$

where the zero in W_V denotes a zero column vector of length n . As a result, in our context, W_V does not contain learnable parameters.

We then define W_Q and W_K as

$$W_Q = \begin{pmatrix} Q \\ 0 \end{pmatrix}, \quad W_K = \begin{pmatrix} K \\ 0 \end{pmatrix},$$

where the matrices Q and K contain the learnable parameters in W_Q and W_K . Here, $Q, K \in \mathbb{R}^{n \times d_k}$, and the zeros in W_Q and W_K denote one zero row.

The one-hot coding of the coordinates in X then extracts Q and K from W_Q and W_K , i.e.,

$$Q = XW_Q, \quad K = XW_K,$$

As a result of our definitions, in the softmax-free linear setting considered in this paper, the low rank factorization QK^T is applied directly to the right-hand side, i.e., defining $u_\theta = \text{Att}(X)$, we obtain

$$u_\theta = (QK^T)V = QK^Tf. \quad (6)$$

The learning task is therefore to find the attention factors such that

$$QK^T \approx A^{-1},$$

where A is the finite-difference Poisson matrix.

Although our numerical experiments are carried out for a one-dimensional elliptic model problem, the construction should not be viewed as being tied to this particular PDE setting. Rather, the model problem provides a controlled setting in which a nonlocal sequence-to-sequence operator is known exactly and can therefore be used to study the effect of hierarchical, domain-decomposition-induced attention. This is relevant more broadly for one-dimensional sequence models, where local interactions and long-range couplings have to be represented simultaneously.

3 Softmax-Free Attention as Low-Rank Inverse

The baseline for our hierarchical attention is the global low-rank linear attention applied to operator learning, i.e.,

$$M_{\theta, \text{global}}^{-1} = QK^T, \quad Q, K \in \mathbb{R}^{n \times r_g}. \quad (7)$$

Applied to a right-hand side f , the predicted solution is

$$u_{\theta} = Q(K^T f); \quad (8)$$

see (6). The operator's rank is limited by the rank parameter denoted r_g .

Remark 2 *Since A^{-1} is symmetric positive definite, one could restrict to a symmetric factorization BB^T . We deliberately do not impose this constraint here. Both the global and the domain-decomposition models use independent factors Q and K . This gives the optimizer a less constrained parameterization while still allowing the learned operator to approximate a symmetric inverse.*

4 Hierarchical Attention by Two-Level Overlapping Schwarz Domain Decomposition

4.1 Overlapping Subdomains and Coarse Hat Functions

The subdomain construction used in the implementation is an algebraic decomposition of the interior degrees of freedom. It therefore differs slightly from an element-based finite element partition, where neighboring subdomains share an interface node before overlap is added to the left and right of the interface.

Let the global index set of the n interior grid points be

$$\mathcal{I} = \{1, \dots, n\}. \quad (9)$$

The set \mathcal{I} is split into N consecutive disjoint index sets of equal size. Then the index sets are enlarged into the neighboring index sets by n_{δ} indices to form the index sets $\mathcal{I}_i, i = 1, \dots, N$ of the overlapping subdomains. As a result, for a choice of n_{δ} , neighboring overlapping subdomains share $2n_{\delta}$ common grid points, provided the neighboring index sets are larger than the overlap, as is the case in the experiments below.

In this construction, there is no center grid point in the overlap. Therefore, among the two indices closest to the center of the overlap, we choose the larger one as the location of the maximum of the corresponding coarse interface-hat function.

Let $n_i = |\mathcal{I}_i|$, and let

$$R_i \in \mathbb{R}^{n_i \times n}$$

denote the Boolean restriction matrix that extracts the degrees of freedom in \mathcal{I}_i from a global vector in \mathbb{R}^n . Equivalently, $R_i u$ is the subvector of u associated with the overlapping subdomain \mathcal{I}_i , while R_i^T extends a local vector by zero to the global index set.

In all numerical experiments, we use an overlap of $n_{\delta} = 2$. Hence, two neighboring overlapping subdomains have $2n_{\delta} = 4$ common grid points.

4.2 Partition of Unity in the Overlap

In the overlap, several subdomains may cover the same degree of freedom. Let m_j be the number of overlapping subdomains containing grid point j . On subdomain i , define the diagonal weight matrix

$$D_i = \text{diag} \left(\frac{1}{m_j} : j \in \mathcal{I}_i \right). \quad (10)$$

In the decompositions used in the experiments below, each grid point in an overlap region is covered by two neighboring subdomains, so that $m_j = 2$ there, while $m_j = 1$ outside the overlap regions.

Then the weights form a discrete partition of unity:

$$\sum_{i=1}^N R_i^T D_i R_i = I. \quad (11)$$

In the experiments below we use the symmetric overlap weighting

$$R_i^T D_i^{1/2} G_i D_i^{1/2} R_i. \quad (12)$$

4.3 Local Attention Blocks

On each of the N overlapping subdomains, we use a local low-rank attention operator

$$G_i = Q_i K_i^T, \quad Q_i, K_i \in \mathbb{R}^{n_i \times r_\ell}, \quad (13)$$

where r_ℓ denotes the rank of the local attention blocks.

The corresponding fine-level operator is

$$M_{\theta, \text{loc}}^{-1} = \sum_{i=1}^N R_i^T D_i^{1/2} Q_i K_i^T D_i^{1/2} R_i. \quad (14)$$

This operator is sparse in the domain-decomposition sense: each learned block acts only on an overlapping subdomain.

4.4 Coarse Attention Block

In Poisson problems, local blocks alone cannot represent global low-frequency components. We therefore add a coarse attention space. Let

$$\Phi \in \mathbb{R}^{n \times n_0} \quad (15)$$

be a coarse interpolation matrix, i.e., Φ interpolates coarse coefficients to the fine grid. Its transpose Φ^T is used as the corresponding restriction to the coarse space.

In the experiments below, Φ consists of interface hat functions; see Figure 4 in the lower rightmost panel. For N subdomains this gives $n_0 = N - 1$ coarse basis functions, one associated with each pair of neighboring disjoint index sets.

We denote the rank of the coarse attention by r_0 . The coarse attention operator is

$$G_0 = Q_0 K_0^T, \quad Q_0, K_0 \in \mathbb{R}^{n_0 \times r_0}. \quad (16)$$

Interpolated to the fine grid, the coarse contribution is

$$M_{\theta, \text{coarse}}^{-1} = \Phi Q_0 K_0^T \Phi^T. \quad (17)$$

4.5 Two-Level Additive Hierarchical Attention Mechanism

Combining the fine and coarse levels gives the proposed hierarchical attention operator

$$M_{\theta, \text{Schwarz}}^{-1} = \Phi Q_0 K_0^T \Phi^T + \sum_{i=1}^N R_i^T D_i^{1/2} Q_i K_i^T D_i^{1/2} R_i. \quad (18)$$

This is the central construction of the paper. It can be interpreted as a two-level additive Schwarz-inspired attention layer. The term ‘‘hierarchical’’ refers to the coexistence of local fine-scale attention blocks and a global coarse attention mechanism.

5 Training Procedure

5.1 Loss Function

For a batch of right-hand sides $f^{(b)}$, the exact solutions are computed as

$$u^{(b)} = A^{-1} f^{(b)}. \quad (19)$$

The model prediction is

$$u_{\theta}^{(b)} = M_{\theta}^{-1} f^{(b)}. \quad (20)$$

A plain mean-squared error (MSE) tends to underweight examples whose true solutions have small amplitude. This is relevant for Poisson problems because high-frequency right-hand sides produce solutions whose amplitudes are damped by the inverse Laplacian. We therefore use a sample-wise weighted MSE (wMSE)

$$\mathcal{L}_{\text{wMSE}}(\theta) = \frac{1}{B} \sum_{b=1}^B \frac{n^{-1} \|u_{\theta}^{(b)} - u^{(b)}\|_2^2}{\max\{n^{-1} \|u^{(b)}\|_2^2, \varepsilon\}}. \quad (21)$$

where B denotes the batch size and $u_{\theta}^{(b)}$ and $u^{(b)}$ denote the predicted and exact solutions for sample b , respectively.

All our experiments use this loss, setting $\varepsilon = 1e - 30$. Without this weighting, good approximations are not achieved for high frequency right-hand sides.

5.2 Initialization of the Attention Factors

All trainable attention factors are initialized with the same naive random factor initialization. Each independent Q - and K -factor is filled entrywise with normally distributed random numbers multiplied by 0.02. This applies equally to the global attention factors, to all local subdomain factors, and to the coarse attention factors. No problem-dependent initialization is used in the experiments reported here. The optimizer is AdamW with zero weight decay.

5.3 Synthetic Right-Hand Sides

The training data are generated on the fly; no finite stored training set is used. We sample right-hand sides from a mixed Fourier family and normalize each generated right-hand side to unit Euclidean norm. The experiments use the first 16 sine modes and also the first 16 cosine modes on the interior grid points.

The mixed Fourier generator combines two types of right-hand sides in each batch. One half of the batch consists of pure Fourier modes: a single normalized sine or cosine mode is selected and multiplied by a random sign. These pure modes are not damped by a decay factor. The other half consists of random Fourier combinations. In this part, sine and cosine modes $m = 1, \dots, 16$ are combined, with higher modes damped by the factor $m^{-1.5}$. After concatenating the two parts, the batch is shuffled and every right-hand side is normalized.

The global attention model and the hierarchical domain-decomposition attention model see the same sequence of training right-hand sides. We use 16 evaluation right-hand sides in the solution plots, they are generated once with a fixed test seed and are then used for all models.

For each generated right-hand side, the reference solution is computed by applying the exact discrete inverse,

$$u^{(b)} = A^{-1} f^{(b)}.$$

The following code defines the generator used for our mixed Fourier right-hand sides. It was extracted from our more general implementation with the assistance of ChatGPT 5.5 and subsequently verified by hand to produce identical results.

```

1 def normalize_rows(v: torch.Tensor, eps: float = 1.0e-12) -> torch.Tensor:
2     return v / (v.norm(dim=-1, keepdim=True) + eps)
3
4 def fourier_basis(x: torch.Tensor, modes: int) -> torch.Tensor:

```

```

5  """Rows are normalized sine/cosine Fourier modes without decay."""
6  rows = []
7  for m in range(1, modes + 1):
8      rows.append(torch.sin(math.pi * m * x))
9      rows.append(torch.cos(math.pi * m * x))
10     return normalize_rows(torch.stack(rows, dim=0))
11
12 def sample_mixed_fourier_rhs(batch_size: int, x: torch.Tensor) -> torch.Tensor:
13     """Mixed Fourier RHS: half pure modes, half random decaying combinations."""
14     n = x.numel()
15
16     def pure_modes(bs: int) -> torch.Tensor:
17         B = fourier_basis(x, MODES)
18         idx = torch.randint(0, B.shape[0], (bs,), device=DEVICE)
19         signs = 2.0 * torch.randint(0, 2, (bs, 1), device=DEVICE, dtype=DTYPE) - 1.0
20         return signs * B[idx, :]
21
22     def random_combinations(bs: int) -> torch.Tensor:
23         f = torch.zeros(bs, n, device=DEVICE, dtype=DTYPE)
24         for m in range(1, MODES + 1):
25             scale = 1.0 / (m ** DECAy)
26             a = torch.randn(bs, 1, device=DEVICE, dtype=DTYPE) * scale
27             b = torch.randn(bs, 1, device=DEVICE, dtype=DTYPE) * scale
28             f = f + a * torch.sin(math.pi * m * x)[None, :]
29             f = f + b * torch.cos(math.pi * m * x)[None, :]
30         return f
31
32     b1 = batch_size // 2
33     b2 = batch_size - b1
34     f = torch.cat([pure_modes(b1), random_combinations(b2)], dim=0)
35     f = f[torch.randperm(batch_size, device=DEVICE)]
36     return normalize_rows(f)

```

Remark 3 *The distribution of right-hand sides is an essential part of our operator-learning problem. A low-rank attention operator cannot be expected to approximate the inverse Poisson operator uniformly well for all possible right-hand sides if the chosen ranks are much smaller than the problem dimension. In particular, if the training distribution contained all discrete modes with comparable importance and one required uniformly small relative errors for all of them, ranks close to the full dimension would in general be necessary. The mixed Fourier distribution used here is therefore a controlled test class. The pure Fourier modes probe individual frequencies, while the randomly weighted Fourier combinations with algebraically decaying coefficients emphasize smoother right-hand sides but still contain contributions from higher modes. Thus the chosen ranks r_ℓ and r_0 should be understood in relation to this choice of right-hand-sides. The goal is not to learn a uniformly accurate inverse on the complete space \mathbb{R}^n , but to compare global low-rank attention and Schwarz attention on a given class of right-hand sides with both local and global structure.*

6 First Experimental Setup

The main learning-rate sweep uses a problem size of $n = 256$ and $N = 8$ subdomains, we always use an overlap of $n_\delta = 2$, and the local ranks are set to $r_\ell = 4$, the coarse rank is set to $r_0 = 8$. The rank of the global attention operator, which is our baseline, is set to $r_g = 40$. The coarse basis is the interface-hat basis. Since $N = 8$, the dimension of the coarse space is $n_0 = N - 1 = 7$.

The inner dimension of the coarse QK^T factorization is thus automatically set to $r_0 = 7$. Any larger user-specified coarse rank is automatically truncated. For consistency, however, all figures and tables report the user-specified coarse rank, which in this case is 8. This behavior results from the generic implementation of the coarse space, which also supports alternative coarse bases, such as hat functions defined on a grid independent of the domain decomposition and partition-of-unity (PoU) basis functions. Since these alternatives did not outperform the simple interface-hat basis in our experiments, they are not discussed further in this paper. The global rank $r_g = 40$ is chosen to be equal to the nominal rank budget $Nr_\ell + r_0 = 8 \times 4 + 8$.

For the global baseline the parameter count is

$$2nr_g = 2 \cdot 256 \cdot 40 = 20480. \quad (22)$$

For the domain-decomposition attention model, the $N = 8$ local subdomain sizes are

$$n_i = 34, 36, 36, 36, 36, 36, 36, 34, \quad (23)$$

so that $\sum_i n_i = 284$. The local blocks therefore contain

$$2r_\ell \sum_i n_i = 2 \cdot 4 \cdot 284 = 2272 \quad (24)$$

parameters. The coarse block has dimension and rank $r_0 = 7$, giving

$$2 \cdot 7 \cdot 7 = 98 \quad (25)$$

additional parameters. Thus the two-level domain-decomposition attention model has

$$2272 + 98 = 2370 \quad (26)$$

trainable parameters. In this representative configuration the global baseline therefore uses about 8.6 times as many trainable parameters.

We stress again that this is not a parameter-matched comparison: the global model has 20480 trainable parameters, whereas the hierarchical domain-decomposition model has 2370 trainable parameters. The comparison is deliberately favorable to the global baseline in terms of trainable parameter count.

We will also report on a global rank $r_g = 5$, to approximately match the numbers of parameters.

6.1 Learning-Rate Sweep

The learning-rate sweep is generated with the following script.

```

1 mkdir -p runs_lr
2
3 for lr in 1e-4 3e-4 1e-3 3e-3 1e-2 3e-2; do
4   lr_tag=$(echo "$lr" | sed 's/-/m/g; s/+//g; s/\./p/g')
5   python3 compare_global_vs_schwarz.py \
6     --n 256 --subdomains 8 --overlap 2 \
7     --local-rank 4 --coarse-rank 8 \
8     --global-rank 40 \
9     --rhs-mode mixed_fourier \
10    --partition symmetric \
11    --loss weighted_mse \
12    --steps 2000 \
13    --coarse-basis interface_hats \
14    --lr "$lr" \
15    --save-prefix "runs_lr/compare_qkt_lr_${lr_tag}" \
16    --seed 0 --train-seed 4711 --test-seed 4712
17 done

```

Note again that both models use the same naive random factor initialization scale; see section 5.2. Differences in the initial loss therefore result from the different operator structures rather than from different random scales.

Figure 1 shows the training curves for six learning rates. Each panel compares the global low-rank attention baseline with the domain-decomposition attention model.

Figure 1 presents the training histories for the learning rates

$$\eta \in \{10^{-4}, 3 \cdot 10^{-4}, 10^{-3}, 3 \cdot 10^{-3}, 10^{-2}, 3 \cdot 10^{-2}\}.$$

For all learning rates considered, the hierarchical domain-decomposition attention model converges significantly faster than the global low-rank attention baseline. Moreover, the domain-decomposition model consistently reaches a substantially lower final weighted MSE. The advantage is particularly pronounced for moderate learning rates between 10^{-3} and 10^{-2} , where the hierarchical model exhibits both rapid convergence and stable optimization behavior.

Table 1 summarizes the learning-rate sweep. The choice $\eta = 1e - 3$ is most favorable for the global attention model with respect to the final weighted MSE. For the comparison in the next section, we thus use the

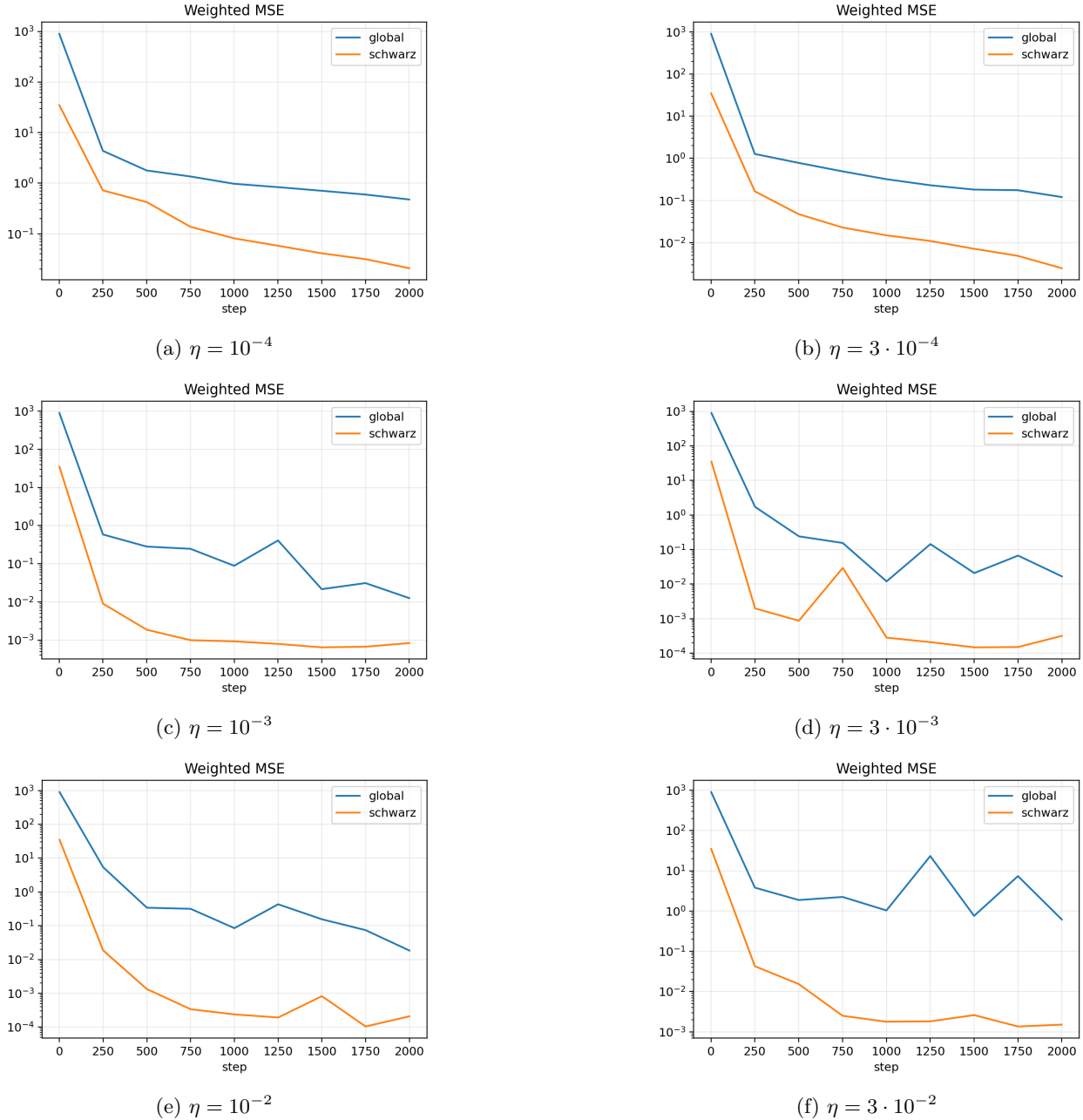


Figure 1: Learning-rate sweep for global low-rank attention and hierarchical domain-decomposition attention. Each panel shows the weighted training MSE on the current training batch. The same training right-hand-side sequence is used for both models. For global attention the lowest weighted MSE at 2000 steps is $1.256e - 2$ and achieved for a learning rate of $\eta = 10^{-3}$. For $\eta = 10^{-3}$ the two-level Schwarz attention has a weighted MSE of $8.319e - 04$ at 2000 steps.

learning rate $\eta = 10^{-3}$. We stress that this choice is deliberately conservative since it is not the best choice for the two-level overlapping Schwarz attention.

Table 2 summarizes the resulting approximation errors for a comparison of global attention and Schwarz attention for $\eta = 1e - 3$: Despite using only 2370 trainable parameters compared to 20480 parameters for the global attention model, the hierarchical domain-decomposition attention achieves a mean relative L^2 error of 2.172×10^{-2} , compared to 6.334×10^{-2} for the global baseline. The maximum relative L^2 error is reduced

Learning rate η	Model	Final weighted MSE	Mean rel. L^2	Max rel. L^2	Rel. op. Frobenius
10^{-4}	Global	$4.760 \cdot 10^{-1}$	$7.280 \cdot 10^{-1}$	$9.755 \cdot 10^{-1}$	5.500
10^{-4}	Schwarz	$2.085 \cdot 10^{-2}$	$1.241 \cdot 10^{-1}$	$3.323 \cdot 10^{-1}$	$6.394 \cdot 10^{-1}$
$3 \cdot 10^{-4}$	Global	$1.208 \cdot 10^{-1}$	$2.785 \cdot 10^{-1}$	$7.486 \cdot 10^{-1}$	5.452
$3 \cdot 10^{-4}$	Schwarz	$2.481 \cdot 10^{-3}$	$4.241 \cdot 10^{-2}$	$1.114 \cdot 10^{-1}$	$6.063 \cdot 10^{-1}$
10^{-3}	Global	$1.256 \cdot 10^{-2}$	$6.334 \cdot 10^{-2}$	$2.231 \cdot 10^{-1}$	3.676
10^{-3}	Schwarz	$8.319 \cdot 10^{-4}$	$2.172 \cdot 10^{-2}$	$6.142 \cdot 10^{-2}$	$4.995 \cdot 10^{-1}$
$3 \cdot 10^{-3}$	Global	$1.669 \cdot 10^{-2}$	$4.427 \cdot 10^{-2}$	$1.339 \cdot 10^{-1}$	1.581
$3 \cdot 10^{-3}$	Schwarz	$3.177 \cdot 10^{-4}$	$9.978 \cdot 10^{-3}$	$2.818 \cdot 10^{-2}$	$3.124 \cdot 10^{-1}$
10^{-2}	Global	$1.842 \cdot 10^{-2}$	$1.586 \cdot 10^{-1}$	1.141	3.069
10^{-2}	Schwarz	$2.085 \cdot 10^{-4}$	$1.158 \cdot 10^{-2}$	$3.881 \cdot 10^{-2}$	$2.868 \cdot 10^{-1}$
$3 \cdot 10^{-2}$	Global	$6.157 \cdot 10^{-1}$	$7.965 \cdot 10^{-1}$	$9.058 \cdot 10^{-1}$	10.27
$3 \cdot 10^{-2}$	Schwarz	$1.513 \cdot 10^{-3}$	$1.775 \cdot 10^{-2}$	$5.676 \cdot 10^{-2}$	$6.779 \cdot 10^{-1}$

Table 1: Summary of the learning-rate sweep using 2000 steps. The final weighted MSE is the last logged value of the training loss. The relative L^2 errors are evaluated on the fixed set of 16 evaluation right-hand sides. The operator error is $\|M_\theta^{-1} - A^{-1}\|_F / \|A^{-1}\|_F$. The best final weighted MSE for the global attention (marked in **bold face**) was observed for the learning rate $\eta = 1e - 3$. The best final weighted MSE for the Schwarz attention (marked in **bold face**) was $\eta = 1e - 2$.

Model	Parameters	Mean rel. L^2 on 16 RHS	Max rel. L^2 on 16 RHS	Rel. Frobenius op. error
Global	20480	$6.334e - 2$	$2.231e - 1$	3.676
Schwarz	2370	$2.172e - 2$	$6.142e - 2$	$4.995e - 1$

Table 2: Quantitative comparison at the learning rate $\eta = 10^{-3}$. The relative L^2 errors are computed on the fixed set of 16 visualization right-hand sides. The operator error is $\|M_\theta^{-1} - A^{-1}\|_F / \|A^{-1}\|_F$. Despite using approximately 8.6 times fewer trainable parameters, the hierarchical Schwarz attention reduces the relative Frobenius operator error from 3.676 to 0.4995.

from 2.231×10^{-1} to 6.142×10^{-2} . The improvement is even more pronounced at the operator level, where the relative Frobenius error decreases from 3.676 to 4.995×10^{-1} .

These results indicate that the domain-decomposition structure is highly effective for learning the inverse Poisson operator in our context. The combination of local low-rank attention blocks with a coarse attention space yields, both, higher approximation accuracy and substantially improved parameter efficiency.

Remark 4 *The relative Frobenius error shown in Table 1 and Table 2 is computed from the full matrices. It measures the discrepancy between the learned operator and the exact inverse. It is therefore different from the training objective, which minimizes a sample-wise weighted forward error. In particular, the learned QK^T factors are not computed as a best rank- r approximation of A^{-1} in Frobenius norm. Hence a comparatively large Frobenius error does not contradict small relative solution errors on the right-hand sides used for evaluation.*

6.2 Approximation Quality on Fixed Visualization Examples

Figures 2 and 3 show the learned approximations for a fixed set of 16 visualization right-hand sides and for the selected learning rate $\eta = 10^{-3}$. These right-hand sides are sampled from the same prescribed distribution as the training right-hand sides, but using a different random seed, and are kept fixed in order to make the visual comparison reproducible.

The purpose of these plots is not to assess out-of-distribution generalization. Instead, they provide a diagnostic view of the learned operator on representative samples from the training distribution, analogous to the weighted MSE values shown in the training curves in Figure 1.

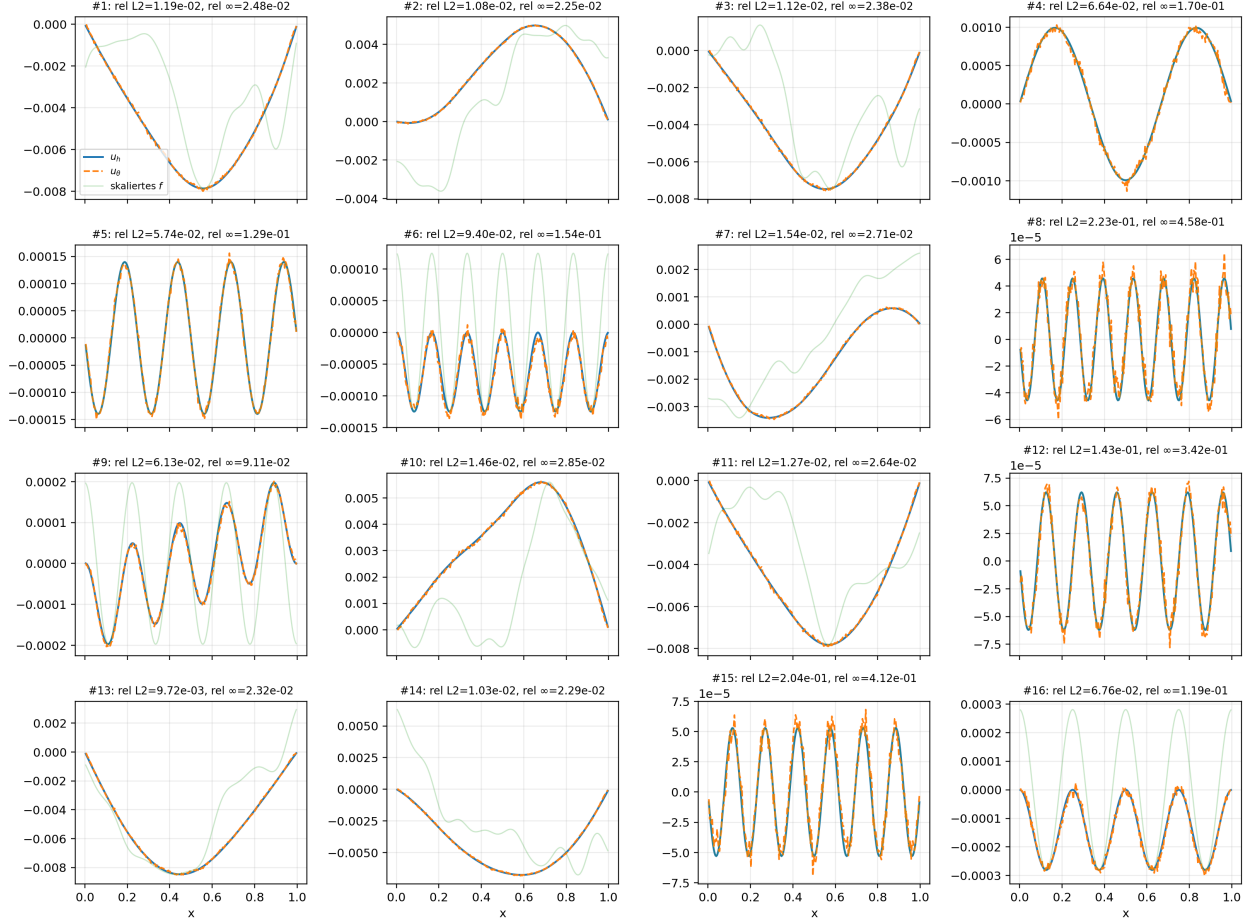


Figure 2: Global low-rank attention on the fixed set of 16 visualization right-hand sides. The model uses $r_g = 40$ and 20480 trainable parameters; $n = 256$, 2000 steps, wMSE loss. Exact solutions $u = A^{-1}f$ (blue) and model predictions (dashed orange) for the 16 fixed evaluation examples. The light green curve shows the right-hand side after panel-wise rescaling, $\tilde{f} = f\|u\|_\infty/\|f\|_\infty$, and is included only to indicate the shape of the right-hand side.

6.3 Visualization of the Learned Operator

The learned operator structure can be inspected by visualizing the global operator, the local domain-decomposition contribution, the coarse contribution, and the full learned operator; see Figure 4. Figure 4 also visualizes the interface hat functions in the lower rightmost panel. In Figure 5 the learned attention blocks are visualized. Figure 6 visualizes the Φ^T -matrix, which collects the hat functions as its rows.

Table 2 summarizes the main comparison of the global attention and the two-level Schwarz attention at the common learning rate $\eta = 10^{-3}$.

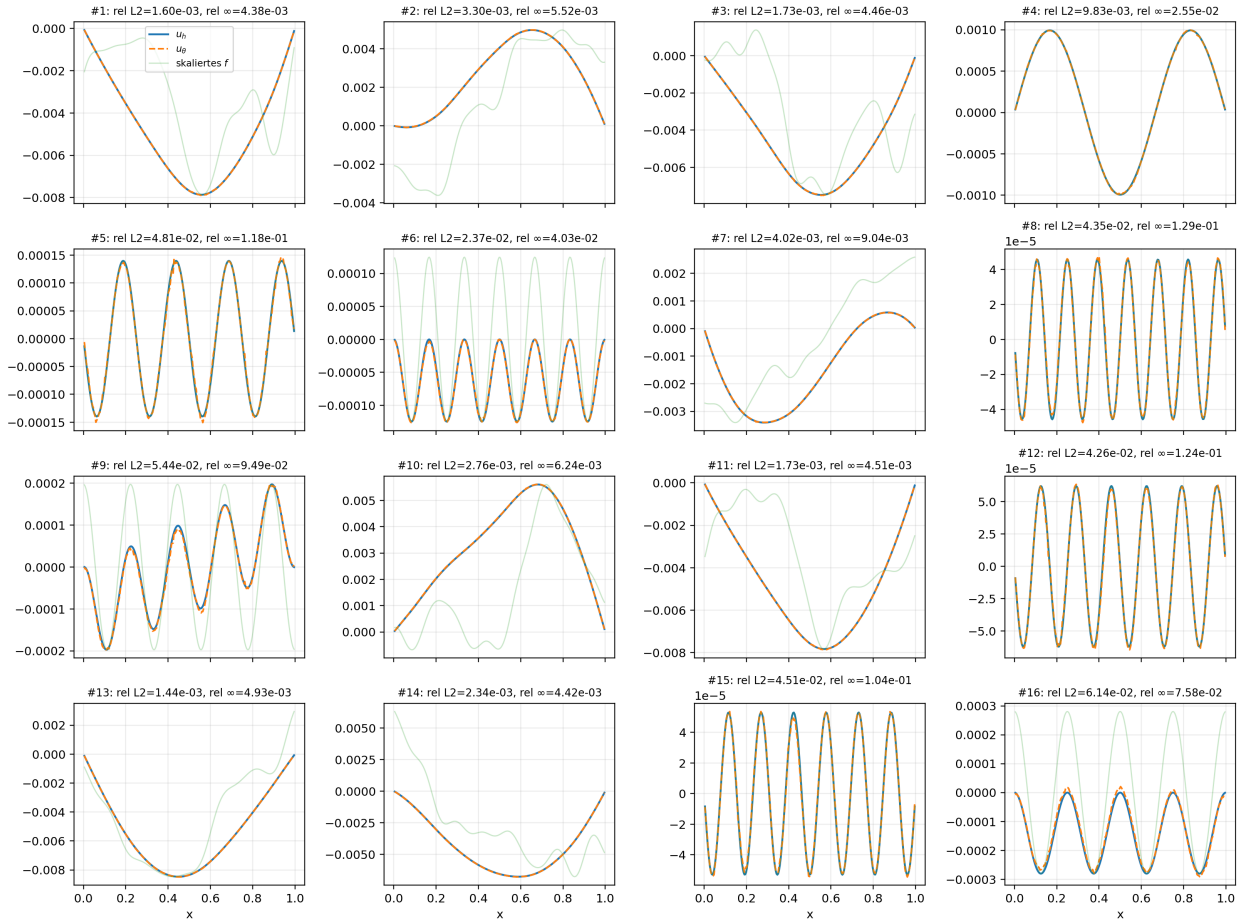


Figure 3: Two-level Schwarz attention on the same fixed set of 16 visualization right-hand sides. The model uses $N = 8$ overlapping subdomains, $n = 256$, local rank $r_\ell = 4$, an interface-hat coarse basis, requested coarse rank $r_0 = 8$, 2000 steps, wMSE loss. This results in 2370 trainable parameters. Exact solutions $u = A^{-1}f$ (blue) and model predictions (dashed orange) for the 16 fixed evaluation examples. The light green curve shows the right-hand side after panel-wise rescaling, $\tilde{f} = f\|u\|_\infty/\|f\|_\infty$, and is included only to indicate the shape of the forcing term.

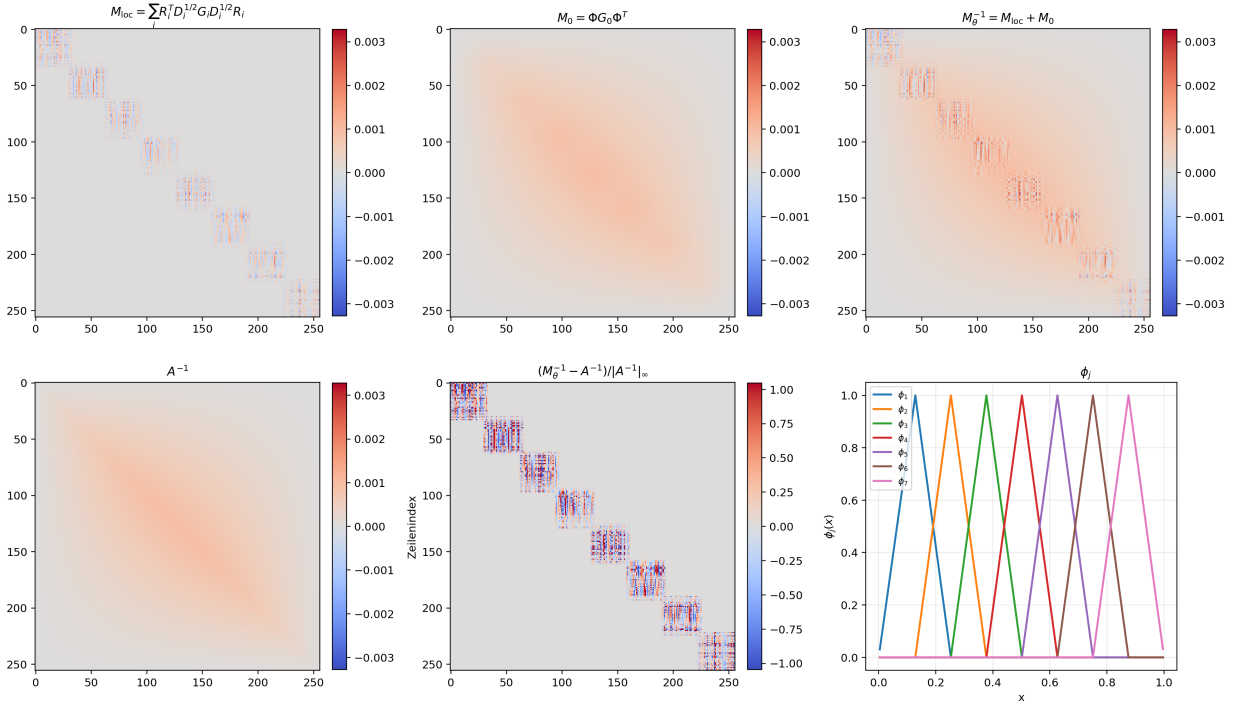


Figure 4: Matrix representation of the learned hierarchical domain-decomposition attention operator. Top row, from left to right: the local overlapping Schwarz contribution $M_{loc} = \sum_i R_i^T D_i^{1/2} G_i D_i^{1/2} R_i$, the coarse contribution $M_0 = \Phi G_0 \Phi^T$, and the full learned operator $M_\theta^{-1} = M_{loc} + M_0$. Bottom row, from left to right: the exact inverse A^{-1} , the normalized error $(M_\theta^{-1} - A^{-1}) / \|A^{-1}\|_\infty$, and the interface-hat coarse basis functions ϕ_j used in the interpolation matrix Φ . The local contribution is block-local due to the subdomain restrictions, whereas the coarse contribution introduces global coupling; hence the assembled two-level operator is generally dense.

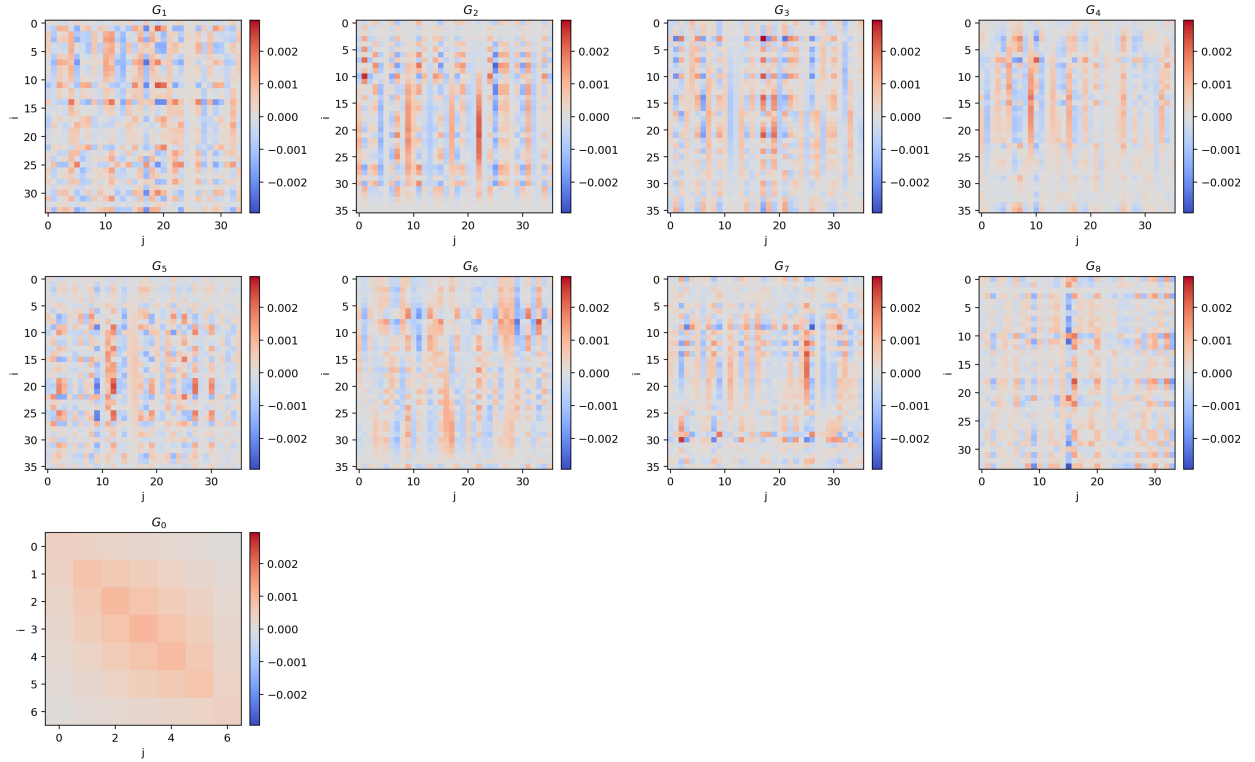


Figure 5: Learned local low-rank attention blocks $G_i = Q_i K_i^T$ and coarse block $G_0 = Q_0 K_0^T$.

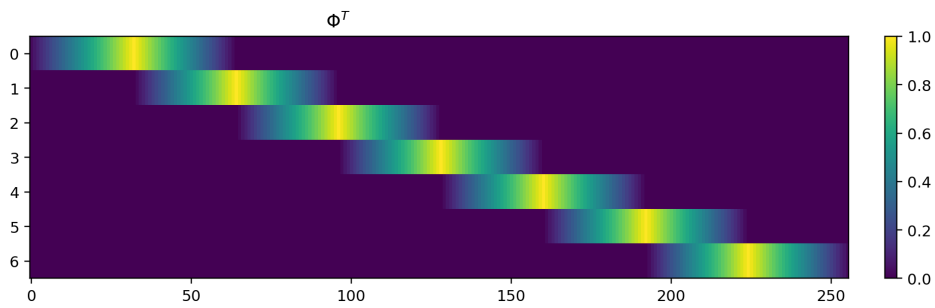


Figure 6: Interface-hat coarse basis used in the restriction matrix Φ^T . For the decomposition into eight disjoint index sets, one hat function is associated with each pair of neighboring index sets, giving seven coarse basis functions. These functions span the coarse space on which the coarse attention block $G_0 = Q_0 K_0^T$ acts before being lifted to the fine grid as $\Phi G_0 \Phi^T$.

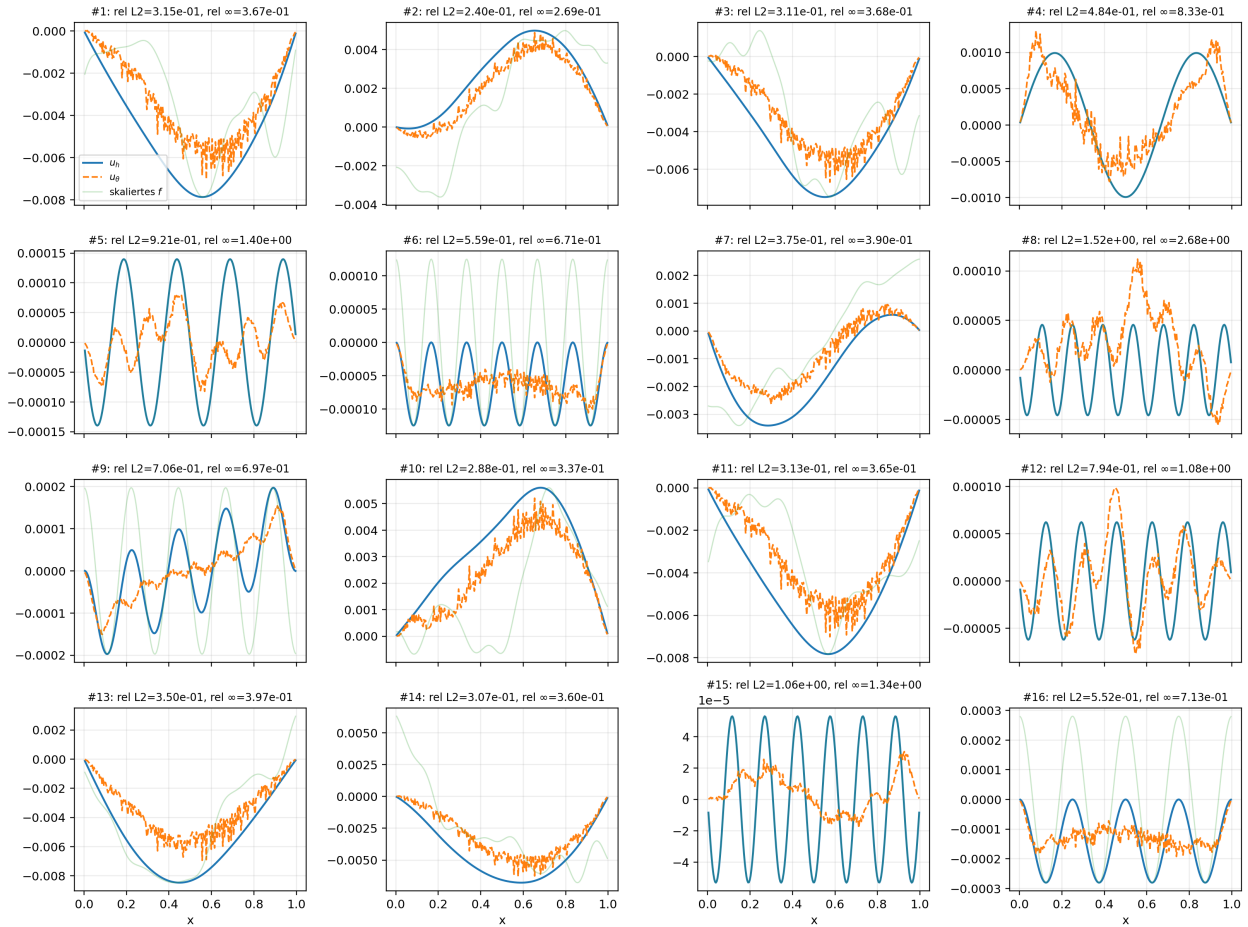


Figure 7: Global low-rank attention on the fixed set of 16 visualization right-hand sides. We use $n = 256$, 2000 steps, wMSE loss. The model uses only global rank $r_g = 5$ and thus 2560 trainable parameters - roughly comparable to the two-level Schwarz case with $N = 8$ subdomains. The final wMSE of this run was $3.410e - 01$, and the approximation quality is visibly low.

7 Increasing the Number of Subdomains

For $N = 16$ subdomains, using $n = 512$, and for $N = 32$ subdomains, using $n = 1024$, we perform additional experiments. We use local ranks $r_\ell = 4$, a requested coarse rank $r_0 = N$, and, for the global attention, $r_g = Nr_\ell + r_0$. We used a learning rate of $\eta = 1e - 2$, which was the best learning rate reported for the Schwarz attention in Table 1 for the case with 8 subdomains and $n = 256$.

Note again that, since the interface hat basis contains only $N - 1$ functions, the coarse QK^T factorization is limited to an inner dimension of $r_0 = N - 1$. Our user-specified coarse rank $r_0 = N$ is therefore automatically truncated to $N - 1$.

In Figure 8, we observe that the Schwarz attention approach continues to train acceptably well for the larger problems, however, the initial weighted training MSE seems to grow with the problem size. This problem needs to be addressed before testing larger numbers of subdomains. Here, it remains to be investigated, whether a simple scaling, e.g., by $1/\sqrt{nd_k}$, can improve this behavior.

Figures 9 and 10 visualize the results for the 16 test right-hand sides. While the quality of the approximations in Figure 9 is good by visual inspection, the approximation in Figure 10 has a somewhat lower quality, reflecting the higher final weighted MSE; see Figure 8. This is at least partially the result of the higher initial weighted MSE, indicating that our parameter initialization should be revisited for larger problems.

The global attention does not achieve competitive results here; see Figure 8, and we do not report details here.

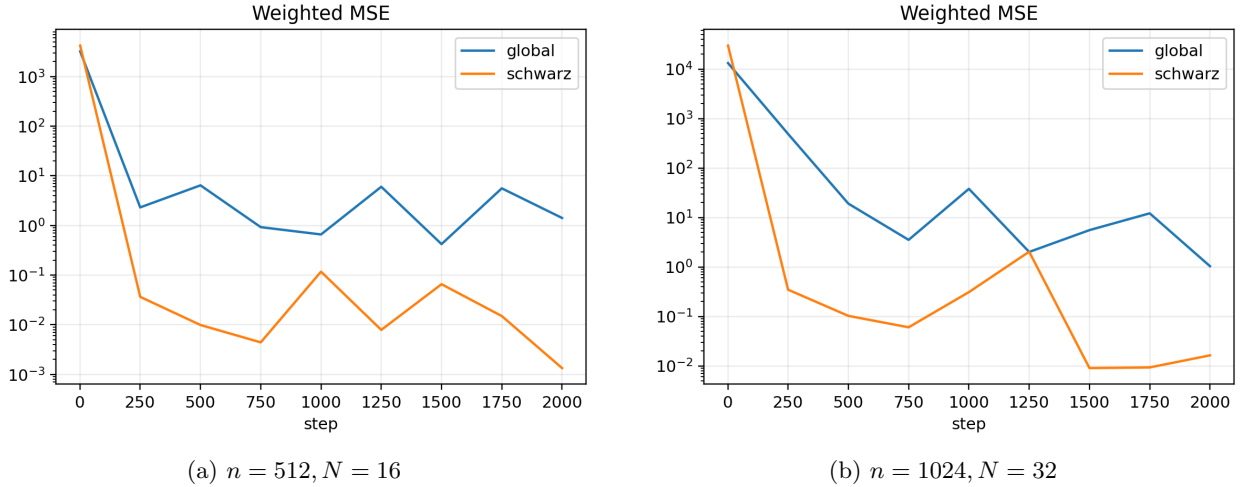


Figure 8: Training curve using $\eta = 1e - 2$ for the problem sizes $n = 512$ and $N = 16$ subdomains (left) and $n = 1024$ and $N = 32$ subdomains (right). For $n = 512$ the training wMSE on the last batch for the Schwarz attention is $1.339e - 03$ and for $n = 1024$ the training wMSE on the last batch for the Schwarz attention is $1.631e - 02$.

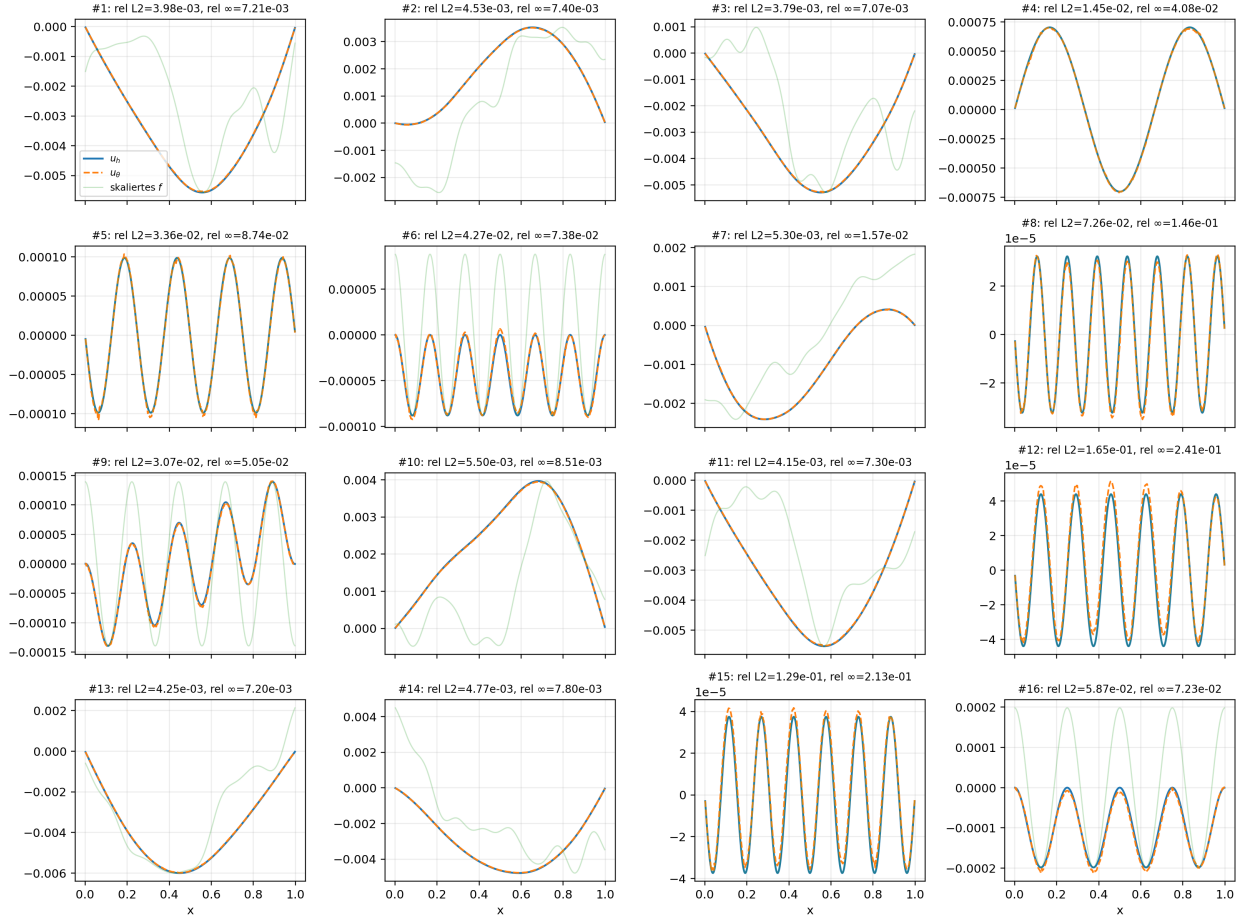


Figure 9: Visualization of the test set for Schwarz attention using $N = 16$ overlapping subdomains, $n = 512$, 2000 steps, wMSE loss, local rank $r_\ell = 4$, requested coarse rank $r_0 = 16$.

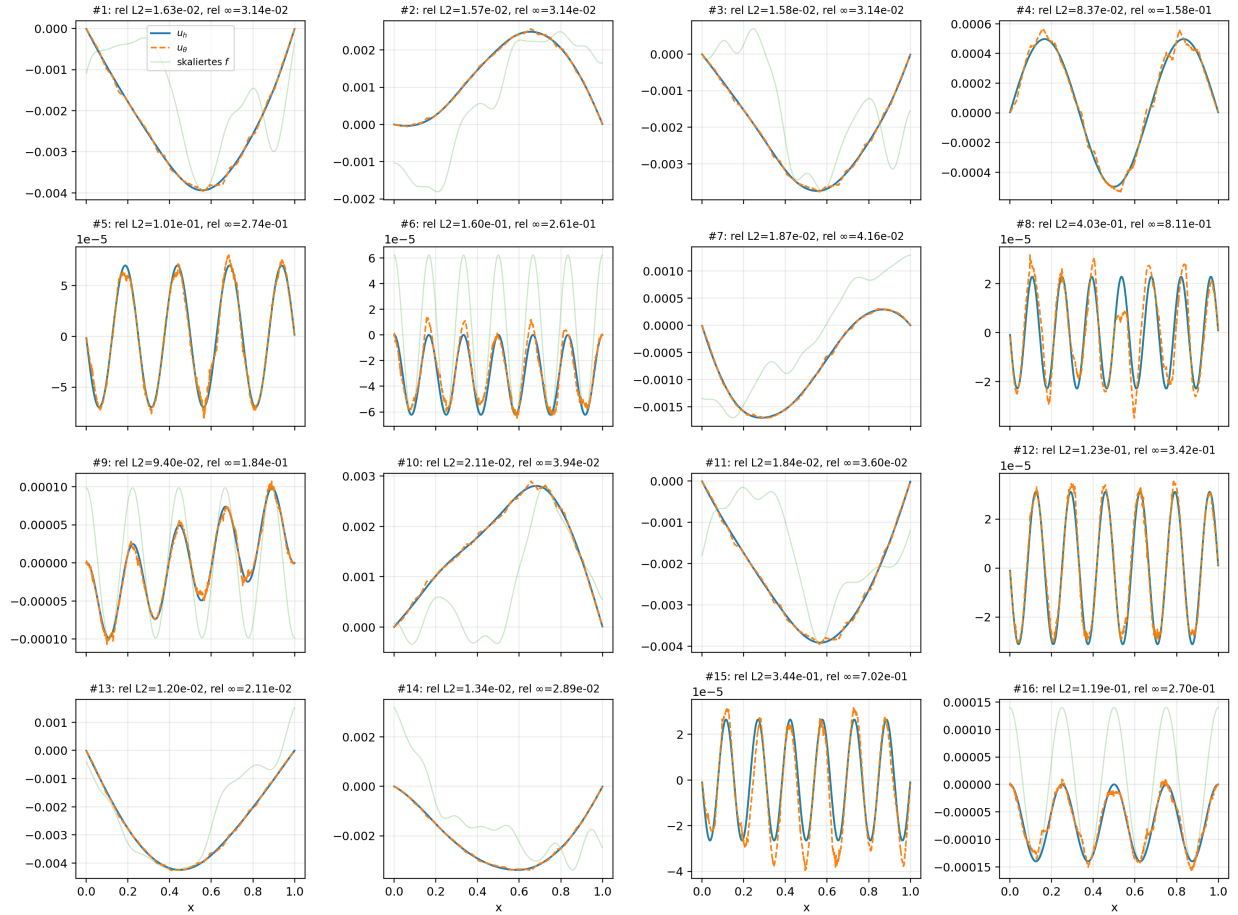


Figure 10: Visualization of the test set for Schwarz attention using $N = 32$ overlapping subdomains, $n = 1024$, 2000 steps, wMSE loss, local rank $r_\ell = 4$, requested coarse rank $r_0 = 32$.

8 Discussion

The experiments support three observations. First, the two-level domain-decomposition attention operator provides a useful structure for the Poisson inverse. The local blocks are intended to capture strong short-range interactions, while the coarse block captures weaker long-range interactions. This mirrors the role of fine and coarse spaces in classical two-level Schwarz methods for elliptic partial differential equations.

Second, the proposed model can be substantially more parameter-efficient than a global low-rank attention baseline. In the representative configuration, the global baseline uses 20480 trainable parameters, while the domain-decomposition model uses 2370. Nevertheless, the domain-decomposition model trains faster and gives more accurate approximations in the shown experiments.

Third, the learning-rate sweep indicates that the advantage is not limited to a single optimization parameter. For the main visual comparison, we use $\eta = 10^{-3}$, which is favorable for the global baseline. The Schwarz attention remains competitive at this learning rate and improves further for slightly larger learning rates. A rate of $\eta = 10^{-2}$ was best for $N = 8$ subdomains and continued to give acceptable results for 16 and 32 subdomains. However, the initial weighted MSE increased with the problem size, indicating that we should revisit the initialization of the QK^T factors before we scale to larger problems.

There are several limitations. The experiments are restricted to a one-dimensional Poisson problem and synthetic Fourier right-hand sides. The model is linear and softmax-free. This is intentional for the present study: it isolates the effect of domain-decomposition structure. Extensions to nonlinear PDEs, higher-dimensional grids, finite element discretizations, and nonlinear attention architectures, e.g., including softmax, remain future work.

9 Conclusion

We introduced a hierarchical attention mechanism inspired by two-level overlapping Schwarz domain decomposition. The method replaces a dense global low-rank attention operator by a sum of local overlapping attention blocks and a coarse attention block. For the one-dimensional Poisson inverse, this construction gives a compact and interpretable operator-learning model. The numerical results suggest that domain-decomposition structure can improve both parameter efficiency and training behavior in softmax-free operator learning, where a global attention is the baseline.

Note on AI Use

Large language models, including ChatGPT 5.5 and Anthropic’s Claude Fable 5, a publicly available Mythos-class model at the time of writing, were used to assist in the development of two independent Python prototypes of the methods discussed in this paper. The authors reviewed, tested, debugged, and iteratively refined the generated code. The numerical experiments reported here were performed with one of these prototypes and checked against the independently developed second prototype. ChatGPT was also used to support the preparation of the manuscript, in particular to improve wording, structure, and presentation.

References

- [1] Ashish Vaswani, Noam Shazeer, Niki Parmar, Jakob Uszkoreit, Llion Jones, Aidan N. Gomez, Łukasz Kaiser, and Illia Polosukhin. Attention is all you need. In I. Guyon, U. V. Luxburg, S. Bengio, H. Wallach, R. Fergus, S. Vishwanathan, and R. Garnett, editors, *Advances in Neural Information Processing Systems*, volume 30. Curran Associates, Inc., 2017.
- [2] Diederik P. Kingma and Jimmy Ba. Adam: A method for stochastic optimization. *arXiv preprint arXiv:1412.6980*, 2014.
- [3] Andrea Toselli and Olof Widlund. *Domain Decomposition Methods – Algorithms and Theory*, volume 34 of *Springer Series in Computational Mathematics*. Springer, Berlin, Heidelberg, 2005.
- [4] Barry F. Smith, Petter E. Bjørstad, and William D. Gropp. *Domain Decomposition: Parallel Multilevel Methods for Elliptic Partial Differential Equations*. Cambridge University Press, Cambridge, 1996.
- [5] Pierre-Louis Lions. On the Schwarz alternating method. I. In Roland Glowinski, Gene H. Golub, Gérard A. Meurant, and Jacques Périaux, editors, *First International Symposium on Domain Decomposition Methods for Partial Differential Equations*, Philadelphia, PA, 1988. SIAM.

- [6] Jae Yong Lee, Seungchan Ko, and Youngjoon Hong. Finite element operator network for solving elliptic-type parametric PDEs. *SIAM Journal on Scientific Computing*, 47(2):C501–C528, 2025. doi:10.1137/23M1623707. URL <https://doi.org/10.1137/23M1623707>.
- [7] Lu Lu, Pengzhan Jin, Guofei Pang, Zhongqiang Zhang, and George Em Karniadakis. Learning nonlinear operators via DeepONet based on the universal approximation theorem of operators. *Nature Machine Intelligence*, 3:218–229, 2021. doi:10.1038/s42256-021-00302-5.
- [8] Zongyi Li, Nikola Kovachki, Kamyar Azizzadenesheli, Burigede Liu, Kaushik Bhattacharya, Andrew Stuart, and Anima Anandkumar. Fourier neural operator for parametric partial differential equations. In *International Conference on Learning Representations*, 2021.
- [9] Pierre Jolivet, Frédéric Hecht, Frédéric Nataf, and Christophe Prud’homme. Scalable domain decomposition preconditioners for heterogeneous elliptic problems. In *Proceedings of the International Conference on High Performance Computing, Networking, Storage and Analysis (SC ’12)*, Washington, DC, USA, 2012. IEEE Computer Society. doi:10.1109/SC.2012.80.
- [10] Alexander Heinlein, Oliver Rheinbach, and Friederike Röver. Parallel scalability of three-level FROSch preconditioners to 220000 cores using the Theta supercomputer. *SIAM Journal on Scientific Computing*, 44(4):C253–C278, 2022. doi:10.1137/21M1431205.
- [11] Saeed Amizadeh, Sara Abdali, Yinheng Li, and Kazuhito Koishida. Hierarchical self-attention: Generalizing neural attention mechanics to multi-scale problems. In *Advances in Neural Information Processing Systems (NeurIPS)*, 2025. doi:10.48550/arXiv.2509.15448. arXiv:2509.15448.
- [12] Chengxi Han, Chen Wu, Haonan Guo, Meiqi Hu, and Hongruixuan Chen. HANet: A hierarchical attention network for change detection with bi-temporal very-high-resolution remote sensing images. *IEEE Journal of Selected Topics in Applied Earth Observations and Remote Sensing*, 16:3867–3883, 2023. doi:10.1109/JSTARS.2023.3264802.
- [13] Paul Hongsuck Seo, Zhe Lin, Scott Cohen, Xiaohui Shen, and Bohyung Han. Progressive attention networks for visual attribute prediction. *arXiv preprint arXiv:1606.02393*, 2016. doi:10.48550/arXiv.1606.02393.
- [14] Haoyu He, Markus Flicke, Jan Buchmann, Iryna Gurevych, and Andreas Geiger. HDT: Hierarchical document transformer. *arXiv preprint arXiv:2407.08330*, 2024. doi:10.48550/arXiv.2407.08330. Published at COLM 2024.
- [15] Ilias Chalkidis, Xiang Dai, Manos Fergadiotis, Prodromos Malakasiotis, and Desmond Elliott. An exploration of hierarchical attention transformers for efficient long document classification. *arXiv preprint arXiv:2210.05529*, 2022. doi:10.48550/arXiv.2210.05529.
- [16] Yongli Hu, Puman Chen, Tengfei Liu, Junbin Gao, Yanfeng Sun, and Baocai Yin. Hierarchical attention transformer networks for long document classification. In *2021 International Joint Conference on Neural Networks (IJCNN)*, pages 1–7, 2021. doi:10.1109/IJCNN52387.2021.9534365.
- [17] Zichao Yang, Diyi Yang, Chris Dyer, Xiaodong He, Alex Smola, and Eduard Hovy. Hierarchical attention networks for document classification. In *Proceedings of the 2016 Conference of the North American Chapter of the Association for Computational Linguistics: Human Language Technologies*, pages 1480–1489, San Diego, California, 2016. Association for Computational Linguistics. doi:10.18653/v1/N16-1174.
- [18] Shuhao Cao. Choose a transformer: Fourier or Galerkin. In *Advances in Neural Information Processing Systems*, volume 34, pages 24924–24940, 2021. URL <https://proceedings.neurips.cc/paper/2021/file/d0921d442ee91b896ad95059d13df618-Paper.pdf>. arXiv:2105.14995.